Spiral Fat Arcs – Bounding Regions with Cubic Convergence

Michael Bartoň[a], Gershon Elber[a]

[a] *Technion – Israel Institute of Technology, Haifa 32000, Israel*

Abstract

A bounding region for spiral curve segments shaped by two circular arcs, parts of the osculating circles at the spiral's endpoints, and two lines is introduced. This bounding region, denoted Spiral Fat Arc ($\mathcal{SFA}$) is simple to construct and process, and shows a cubic approximation order to a given spiral curve.

Given a general planar parametric curve, it can be split at curvature extrema (and inflection points), solving for the parametric locations for which $\kappa' = 0$ (and $\kappa = 0$), κ being the signed curvature field, to yield a set of spiral curves. Each of the spirals is then fitted with a bounding $\mathcal{SFA}$.

Finding the intersection locations of two free-form planar curves is a fundamental task in geometric computing and computer aided design, and can immediately benefit from this new $\mathcal{SFA}$ bounding region. A recursive curve-curve intersection (CCI) algorithm that efficiently computes the intersection location of two parametric curves using $\mathcal{SFA}$s is also introduced.

Key words: spiral, monotone curvature, curve-curve intersection, bounding regions, fat-arcs

1. Introduction and Related Work

Spiral curves had become an important tool in geometric modeling and computer-aided design, in the past decades. These curves, possessing a property of a monotone curvature, were focused to be immensely useful due to their eye-pleasing shape [1, 13]. In shape design, a curve is typically required to not only be sufficiently smooth but also of attractive appearance [14]. High order continuity/smoothness need not to be a decisive criterion, when the aesthetic aspect of the curve is taken into account [13]. In computed numerically controlled (CNC) machining, a path of the end-effector may also be required to have monotonous curvature [22].

Hence, curves with monotone curvature, or even more – with monotone change of curvature [19], are starting to be thoroughly investigated. In 2D, a special one-parametric family of spirals represented as *Bézier curves* was introduced [15]. By constraining the length and the angle of two neighboring edges of its control polygon, these curves, known as *typical*, are guaranteed to have

monotone curvature. A construction of a spiral segment that interpolates given G^2 boundary data (endpoints, unit tangents and signed curvatures) was presented in [21]. In order to get more degrees of freedom, *rational* Bézier spirals that interpolate given G^2 data were considered in [7]. Recently, a circular inversion was applied to an arc of a parabola to construct a spiral segment that satisfies G^2 boundary conditions [12].

In 3D, not only the curve's curvature, but also the torsion of the curve needs to be considered. A generalization of the typical curves of [15] into 3D was proposed in [11], yielding a family of space curves with monotone *curvature and torsion*.

The curve-curve intersection problem (CCI) is a fundamental task in computer aided design. Algorithms that efficiently find these points are therefore strongly desirable. *Bounding regions* that contain given curve(s) are commonly used in CCI-algorithms. These bounds are recursively intersected and parts of both curves that lie outside the mutual intersection domains are trimmed away. The *approximation order* of the bounding region to the original curve typically reflects the quality/tightness of the bound. Consequently, this measure determines how quickly the algorithm converges to the desired intersection point, known as *convergence rate*. Naturally, the higher the convergence order is the lower the number of iterations of the algorithm needed. On the other hand, the bounding region is required to be as simple as possible, since it is constructed and intersected in every iteration of the algorithm. Hence, some balance between the convergence order and the simplicity of the bound is to be maintained.

Common bounding regions are bounding boxes, planar strips, fat lines, convex hulls or fat arcs [16, 10, 3, 4]. Such regions are very easy to construct and the intersection requires the solution of (at most) quadratic equation(s). For two Bézier/Bspline curves, a method known as *Bézier clipping* was introduced in [16]. It exploits the convex hull property of these curves and, in single intersections, converges quadratically to the intersection point [18].

Fat arcs, regions bounded by a pair of co-centric circles, were considered in [10] for *parametric* curves. Numerical tests showed cubical convergence rate in single roots. Another scheme that handles *implicit* curves was presented in [3, 2]. An implicit curve is considered as a zero set of a bivariate polynomial over a given 2D box. Using the Bernstein-Bézier representation, the best linear approximation with respect to the L^2 norm, a 3D plane, is constructed. Using bounds on the approximation errors, 3D bounding strips and consequently *fat lines* in 2D are obtained. These two bounding fat lines define a 2D parallelogram, which is afterwards intersected with the original domain and thus the new domain is defined. This scheme converges quadratically to a single root. A generalization, that exploits one linear approximation (fat line) and one quadratic (fat conic), [4] has shown a cubic convergence rate in single roots and superlinear (1.5) in double roots. Recently, an algorithm that generates a collection of bounding fat arcs of a given implicit curve was discussed [5].

In this work, we introduce a bounding region for spiral curve segments whose boundary consists of two circular arcs, parts of the osculating circles at the

spiral's endpoints, and two lines. These bounding regions, denoted *Spiral Fat Arcs* ($\mathcal{SFA}$) are simple to construct, process and present cubic convergence rate.

Given a general parametric curve, it can be split at curvature extrema (and inflection points), solving for the parametric locations for which $\kappa' = 0$ (and $\kappa = 0$), κ being the signed curvature field, to yield a set of spiral curves. It should be noted that if $\varphi(t)$ is a regular piecewise polynomial curve, so will be the zero (numerator) constraints for κ' and κ.

Once both curves are split into spirals, their $\mathcal{SFA}$s are constructed and, if overlap, intersected. Parts of both segments that can not contribute to an intersection point are trimmed away and the process is recursively repeated. Due to the cubic approximation order of a curve by its osculating circle, the algorithm is proved to converge with cubic convergence rate toward a single (transversal) intersection point.

The rest of the paper is organized as follows. In Section 2, a brief summary on spirals is given and $\mathcal{SFA}$ regions are introduced. Section 3 formulates the CCI algorithm and discusses its convergence rate. Several examples are given in Section 4 and finally the paper is concluded in Section 5.

2. Spirals

In this section, we briefly recall the notion of a spiral curve, summarize some of its properties and introduce its simple bounding region, *spiral fat arc*.

Definition 1. The differentiable mapping $\varphi : [0, 1] \to \mathbb{R}^2$ is said to be a *regular spiral curve* if $\|\varphi'(t)\| \neq 0$ and its curvature $\kappa(t)$ is continuous and strictly monotone for all $t \in [0, 1]$.

Remark 1. If no misunderstanding can occur, we title both the mapping and its image by a spiral. In addition, in the rest of the paper, if not stated differently, without loss of generality the curvature is considered strictly increasing (otherwise reverse the parametrization).

2.1. Spirals as envelopes of nested systems of circles

Curvature is a measure of the change of the curve's unit tangent vector [6]. Since a spiral has an increasing curvature, whereas the curvature of its osculating circle is constant, locally a spiral "crosses" its osculating circle. This property is formulated in the following lemma.

Lemma 1. *An osculating circle of spiral φ locally intersects φ only at the osculating point.*

Proof. Let φ be arc-length parameterized curve and let $O(a)$ be the center of the osculating circle of φ, $c(a)$, at some point $\varphi(a)$. Denote by R the radius of osculating circle $R(a) = \|\varphi(a) - O(a)\|$, see Fig. 1, where $\|\cdot\|$ denotes

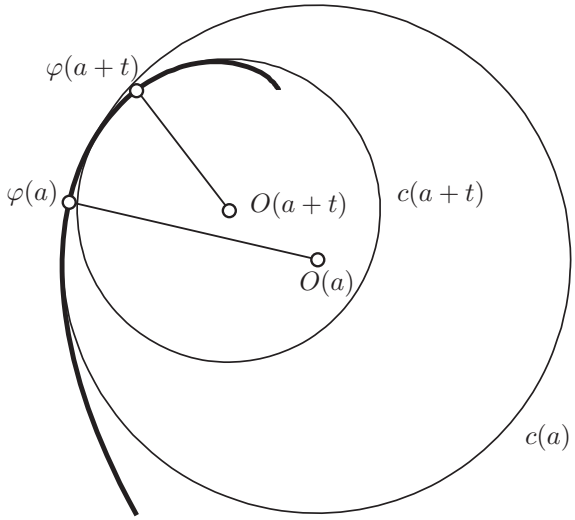

Figure 1: Spiral curve φ and two of its osculating circles, $c(a)$ and $c(a+t)$, from the infinite set of osculating circles, $\mathcal{C}$. $\mathcal{C}$ is ordered with respect to inclusion. φ intersects every osculating circle in $\mathcal{C}$ only at the osculating point.

the Euclidean norm. Let $d(t) = \|\varphi(a+t) - O(a)\|^2 - R(a)^2$. Then, a direct computation gives

$$\begin{aligned} d'(t) &= 2\langle \varphi'(a+t), \varphi(a+t) - O(a)\rangle, \\ d''(t) &= 2\langle \varphi''(a+t), \varphi(a+t) - O(a)\rangle + 2\langle \varphi'(a+t), \varphi'(a+t)\rangle, \\ d'''(t) &= 2\langle \varphi'''(a+t), \varphi(a+t) - O(a)\rangle + 6\langle \varphi''(a+t), \varphi'(a+t)\rangle, \end{aligned} \tag{1}$$

and consequently in the Taylor expansion of d at $t = 0$, the first three terms (a constant, t and t^2) vanish whereas the coefficient of t^3 is non-zero ($2\kappa(a)$). This directly implies the change of the sign of d at 0. □

Definition 2. Let $\varphi(t)$, $t \in [0,1]$, be a spiral and $c(t)$ its osculating circle. The infinite set

$$\mathcal{C} = \{c(t), t \in [0,1]\} \tag{2}$$

is referred to as a *system of osculating circles* of φ.

Definition 3. We say that a one-parameter system of circles (2) is *nested* (ordered with respect to inclusion) if $c(t_2) \subset c(t_1)$ for every $t_1 < t_2, t_1, t_2 \in [0,1]$.

Lemma 2. *System $\mathcal{C}$ of osculating circles along a spiral curve φ is nested.*

Proof. Assume that φ is an arc-length parameterized spiral. Let $c(a)$ and $c(a+t)$, $t > 0$ be two circles of system $\mathcal{C}$ and let $O(a)$ and $O(a+t)$ be their centers, respectively, see Fig. 1. Circle $c(a+t)$ is contained in $c(a)$ if and only if

$$\|O(a) - O(a+t)\| < R(a) - R(a+t), \tag{3}$$

where $R(a) = \|\varphi(a) - O(a)\|$ is the radius of $c(a)$. Define functions

$$\begin{array}{rcl} d_O(t) & = & \|O(a) - O(a+t)\|^2, \\ d_R(t) & = & |R(a) - R(a+t)|^2 \end{array} \tag{4}$$

and observe the Taylor expansion of both $d_O(t)$ and $d_R(t)$ with respect to variable t, at $t = 0$. Similarly to (1), direct computation of the derivatives gives $d_O(0) = 0$, $d'_O(0) = 0$, $d''_O(0) = 2\|O'(a)\|^2$, $d'''_O(0) = 6\langle O''(a), O'(a)\rangle$ and

$$d''''_O(0) \quad = \quad 8\langle O'(a), O'''(a)\rangle + 6\langle O''(a), O''(a)\rangle \tag{5}$$

and analogously for $d_R(t)$ we obtain $d_R(0) = 0$, $d'_R(0) = 0$, $d''_R(0) = 2R'^2(a)$, $d'''_R(0) = 6R'(a)R''(a)$ and

$$d''''_R(0) \quad = \quad 8R'(a)R'''(a) + 6R''^2(a). \tag{6}$$

Since φ is arc-length parameterized, Frenet formulas give $N' = -\kappa\varphi' = -\frac{1}{R}\varphi'$ or

$$\begin{array}{rcl} O & = & \varphi + RN, \\ O' & = & \varphi' + R'N + RN' = R'N, \\ O'' & = & R''N + R'N', \\ O''' & = & R'''N + 2R''N' + R'N'', \end{array} \tag{7}$$

where N denotes the unit normal of φ and κ its curvature. Observe that $d_O^{(i)}(0) = d_R^{(i)}(0)$, $i = 0, \ldots, 3$, but

$$d_O^{(4)}(0) < d_R^{(4)}(0). \tag{8}$$

Using (7) and the fact that φ is a planar curve (its torsion $\tau = 0$), we obtain

$$\begin{array}{rcl} \langle O', O'''\rangle & = & R'R''' - R'^2\kappa^2, \\ \langle O'', O''\rangle & = & R''^2 + R'^2\kappa^2, \end{array} \tag{9}$$

and substituting (9) into Eq. (5), we get an inequality of leading terms of both Taylor expansions, Eq. (8), and consequently $d_O(t) < d_R(t)$ for small $t > 0$.

Since for all a, $c(a) \in \mathcal{C}$ fully contains all $c(a+t)$, $t \in [0, t_0]$ for some $t_0 \in \mathbb{R}^+$, $\mathcal{C}$ is ordered with respect to inclusion. □

Corollary 1. *A spiral is a self-intersection free curve.*

Proof. Let $t_1, t_2 \in [0, 1]$, $t_1 < t_2$, be two parameters of spiral φ. Define $t_M = \frac{t_1+t_2}{2}$ and consider osculating circle $c(t_M)$ of φ at $\varphi(t_M)$. Since $\mathcal{C}$ is nested and φ is osculating to its osculating circle only at the contact point, $c(t_M)$ separates $\varphi(t_1)$ and $\varphi(t_2)$ and hence $\varphi(t_1) \neq \varphi(t_2)$. □

An algorithm to compute self-intersections of a general (planar) curve by splitting it into spiral can also immediately benefit from Corollary 1: 1) Split input curve into spiral segments. 2) Intersect the different spirals. We formulate a curve-curve-intersection algorithm in Section 3. Prior to this, we define a new bounding region of a spiral curve.

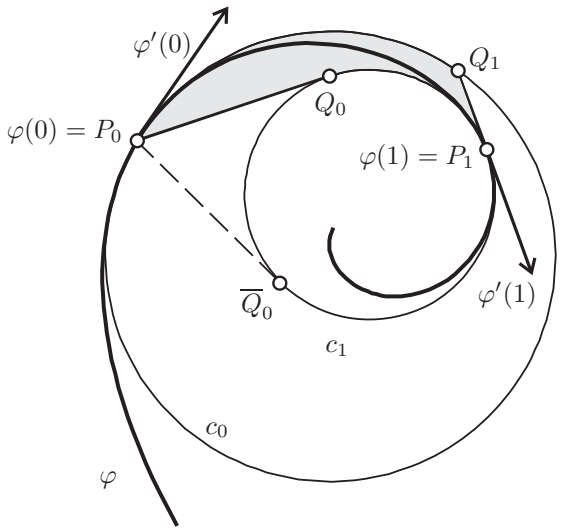

Figure 2: (a) A segment of spiral parametric curve φ between endpoints $\varphi(0) = P_0$ and $\varphi(1)P_1$ is bounded by a spiral fat arc (grey) which is delimited by two straight lines and two circular arcs, $P_0\widehat{Q_1}$ and $Q_0\widehat{P_1}$. Q_0 is the contact point between the tangent of c_1 at P_0, where c_1 is the osculating circle of φ at P_1. Q_1 is the intersection of c_0 with the tangent of c_1 at P_1, in the direction opposite to $\varphi'(1)$, where $\varphi'(1)$ is the common tangent of φ and c_1 at P_1.

2.2. Bounding spiral fat arcs

In this subsection, we introduce an easy-to-construct bounding region of a spiral segment, the *spiral fat arc* ($\mathcal{SFA}$), which fully contains and tightly bounds a given spiral curve. Consider osculating circle c_0, (c_1) of spiral $\varphi(t)$, $t \in [0, 1]$, at the startpoint $\varphi(0) = P_0$ (endpoint $\varphi(1) = P_1$), see Fig 2. Due to Lemma 2, $c_1 \subset c_0$. Further, φ is contained in the circular ring between c_0 and c_1. In addition, let us assume

$$\int_0^1 \kappa(t)dt < 2\pi. \tag{10}$$

Definition 4. Let Q_0 and $\overline{Q}_0$ be the contact points on c_1 and the two tangents of c_1 through point P_0 such that $\langle \varphi'(0), Q_0P_0 \rangle > \langle \varphi'(0), \overline{Q}_0P_0 \rangle$ and let Q_1 be the intersection point between c_0 and the tangent line of c_1 at P_1 such that $\langle \varphi'(1), Q_1P_1 \rangle < 0$, see Fig 2. The region delimited by the two circular arcs, $P_0\widehat{Q_1}$ and $Q_0\widehat{P_1}$, and the two lines $\overline{P_0Q_0}$ and $\overline{P_1Q_1}$ defines the *spiral fat arc* of φ. Arc $P_0\widehat{Q_1}$ together with line Q_1P_1 will be referred to as an *upper envelope* of φ, whereas $Q_0\widehat{P_1}$ and P_0Q_0 define its *lower envelope*.

Observe Inequality (10) is required to guarantee that φ does not possess a loop inside the circular ring. Obviously, if assumption (10) is violated, the

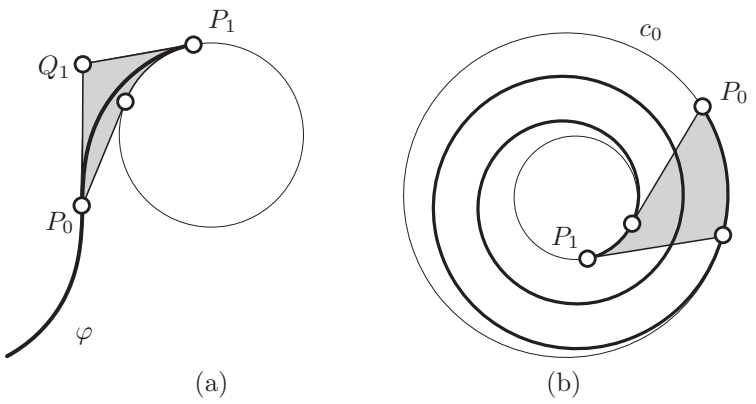

Figure 3: (a) A limit case of a $\mathcal{SFA}$ region at inflection point P_0. The upper envelope of φ consists of two lines P_0Q_1 and Q_1P_1. (b) $\mathcal{SFA}$ region is well defined only for spiral arcs that satisfy ineq. (10).

spiral is not bounded by its $\mathcal{SFA}$, see Fig. 3(b). In such a case, the curve is subdivided and two sub-$\mathcal{SFA}$s are constructed. In order to reduce the number of redundant subdivisions, one can exploit the magnitude on the left side of Inequality (10), which indicates the number of loops, and subdivide the curve directly into several pieces.

Remark 2. If the curvature of φ is (almost) zero, its osculating circle converges to a line and therefore the computation of the osculating circle can be numerically unstable. In such a case, the limit case is directly considered and the arc in the upper envelope of φ is replaced by a segment of tangent line as depicted at Fig. 3(a).

3. Curve-curve intersection using spiral fatarcs

In this section, we introduce an algorithm which exploits the $\mathcal{SFA}$ bounding regions and computes the intersection points of two planar parametric curves. The algorithm isolates all intersection points and, in the transversal intersection case, has a cubical convergence rate.

Definition 5. Let $\varphi_1(t)$, $\varphi_2(s)$, $t, s \in [0,1]$ be two planar parametric curves. We say that $\varphi_i(t)$, $i = 1, 2$, intersect *transversally* at point P if there exist unique parameters $t^\star, s^\star \in [0,1]$ such that $P = \varphi_1(t^\star) = \varphi_2(s^\star)$ and tangent vectors $\varphi_1'(t^\star)$ and $\varphi_2'(s^\star)$ are linearly independent.

Definition 6. We say two spiral fat arcs, $\mathcal{SFA}_1$, $\mathcal{SFA}_2$, intersect transversally, if the upper/lower envelope of $\mathcal{SFA}_1$ intersects the upper/lower envelope of $\mathcal{SFA}_2$ at a single point, see Fig. 4(a).

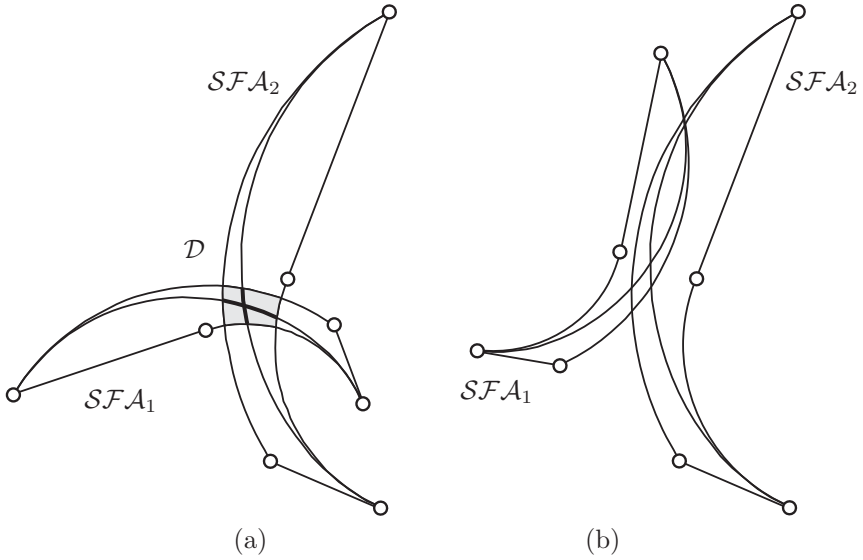

Figure 4: (a) Two spiral fat arcs $\mathcal{SFA}_1$ and $\mathcal{SFA}_2$ in transversal position are intersected and the curve segments are restricted to domain $\mathcal{D}$ (grey). (b) $\mathcal{SFA}$ regions in non-transversal position. In such a case, Algorithm 2 subdivides both curves.

Remark 3. Observe that a spiral curve traverses its $\mathcal{SFA}$ region from one endpoint to another with a monotone curvature (monotone change of its tangent vector). Hence, the transversal intersection of two $\mathcal{SFA}$ regions implies the transversal intersection of two bounded spirals and consequently, there exists a unique intersection point inside the intersected region.

3.1. Algorithm

In order to find an intersection point(s) of two spirals, their $\mathcal{SFA}$s are constructed, mutually intersected, and parts of both curves which lie outside the intersection are trimmed off, see Fig. 4(a). This process, denoted *spiral clipping*, is repeated until some numerical tolerance is reached, see Algorithm 1. This tolerance, ε, might be the diameter of a $\mathcal{SFA}$ or, in our implementation, the range of the two endpoints in the parametric space, see line 12 of Algorithm 1. If the $\mathcal{SFA}$ regions do not intersect, the spirals have no intersection points.

For two general curves, a preconditioning step is required. At this step, both curves are split at points of extremal curvature, $\kappa' = 0$, and at inflection points, $\kappa = 0$, yielding two sets of spiral segments. Since

$$\kappa = \frac{\|\varphi' \times \varphi''\|}{\|\varphi'\|^3}, \tag{11}$$

solving for its roots basically reduces to solve for the roots of a univariate polynomial (numerator of (11)) in the case of a regular rational φ. This is robustly

Algorithm 1 (see Fig. 4) `SpiralClipping`$(\varphi_1, \varphi_2, \varepsilon)$

1: **INPUT**: two spiral curves, $\varphi_1(t)$ and $\varphi_2(s)$;
numerical tolerance ε;

2: $S \leftarrow \emptyset$
3: construct the axis-aligned bounding boxes of both φ_1 and φ_2 to efficiently detect non-overlapping curves;
4: $\mathcal{SFA}_1, \mathcal{SFA}_2 \leftarrow$ construct spiral fat arcs for φ_1 and φ_2;
5: **if** $\mathcal{SFA}_1 \cap \mathcal{SFA}_2 = \emptyset$ **then**
6: **return** S
7: **end if**
8: **if** $\mathcal{SFA}_1$ and $\mathcal{SFA}_2$ intersect transversally **then**
9: $\mathcal{D} \leftarrow \mathcal{SFA}_1 \cap \mathcal{SFA}_2$
10: $[t_0, t_1] \leftarrow$ trim φ_1 by region $\mathcal{D}$;
11: $[s_0, s_1] \leftarrow$ trim φ_2 by region $\mathcal{D}$;
12: **if** $t_1 - t_0 < \varepsilon$ **and** $s_1 - s_0 < \varepsilon$ **then**
13: $t^\star = \frac{t_1 - t_0}{2}$; $s^\star = \frac{s_1 - s_0}{2}$;
14: $S \leftarrow S \cup [t^\star, s^\star]$
15: **else**
16: go to line 3
17: **end if**
18: **else**
19: subdivide in the middle of parametric domains and go to line 3 on all four recursive calls;
20: **end if**
21: **OUTPUT**: S, set of pairs of parametric values $[t^\star, s^\star]$ that approximate the intersection points of φ_1 and φ_2;

achieved by using a numerical solver that guarantees to return *all* roots [8]. Then, spiral clipping is applied to any pair of spiral segments. A whole process is summarized in Algorithm 2.

In the trimming stage, the part of the curve that lies outside the common domain needs to be trimmed off by the boundary of the $\mathcal{SFA}$ region (a line or a circle). Several schemes can be used to achieve this. We use the secant method to iteratively find a conservative intersection point within the prescribed tolerance.

Note that even though the $\mathcal{SFA}$ offers a tight bound on a spiral curve, its construction is more time demanding than the construction of a simple bounding box. In order to improve the timings of Algorithm 1, axis-aligned bounding boxes were used to purge away the non-overlapping parts more efficiently.

3.2. Convergence rate

In order to make this paper self-contained, we formulate following technical lemma.

Algorithm 2 `CurveCurveIntersection`$(\varphi_1, \varphi_2, \varepsilon)$

INPUT: two planar parametric curves φ_1 and φ_2, numerical tolerance ε;

$S \leftarrow \emptyset$

$\{\varphi_1^i\}_{i=1}^m$, $\{\varphi_2^j\}_{j=1}^n \leftarrow$ split both curves into segments with monotone signed curvature; `/* preconditioning stage */`

for $i = 1$ to m **do**

  for $j = 1$ to n **do**

    $S \leftarrow S \cup$ `SpiralClipping`$(\varphi_1^i, \varphi_2^j, \varepsilon)$;

  end for

end for

OUTPUT: S, set of pairs of parametric values that approximate the intersection points of φ_1 and φ_2;

Lemma 3. *Let $c_1(C_1, r_1)$ and $c_2(C_2, r_2)$ be two circles transversally intersected at some point P and let $\mathcal{FA}_1$ ($\mathcal{FA}_2$) be the fat arc arisen from c_1 (c_2) by the offset distance δ such that $\delta \ll r_1, r_2$. Denote by S one of the connected components of $\mathcal{FA}_1 \cap \mathcal{FA}_2$. Then* $\operatorname{diam}(S) = \mathcal{O}(\delta)$.

Proof. See Appendix.

Theorem 1. *Let $\varphi_1(t)$, $\varphi_2(s)$ be two spirals transversally intersected at point P. Then* `SpiralClipping` *converges to P with convergence rate $d = 3$.*

Proof. Let $[t^\star, s^\star]$ be the parameters returned by `SpiralClipping`$(\varphi_1, \varphi_2, \varepsilon)$ that corresponds to P and let $\{[t_0^i, t_1^i] \times [s_0^i, s_1^i]\}_{i=0,1,\ldots}$ be the nested sequence of parametric domains generated by `SpiralClipping` that contain $[t^\star, s^\star]$.

Denote $h_i = \operatorname{diam}([t_0^i, t_1^i] \times [s_0^i, s_1^i])$, the diameter of the parametric domain in the i-th iteration and consider

$$\delta_{1+}^i = \max_{t \in [t_0^i, t_1^i]} (\|\varphi_1(t) - c_{1+}^i\|), \tag{12}$$

$$\delta_{1-}^i = \max_{t \in [t_0^i, t_1^i]} (\|\varphi_1(t) - c_{1-}^i\|), \tag{13}$$

where c_{1+}^i (c_{1-}^i) is the osculating circle of φ_1 at startpoint $\varphi_1(t_0^i)$ (endpoint $\varphi_1(t_1^i)$), see Fig 5. The bounding values of φ_2, δ_{2+}^i and δ_{2-}^i, are defined analogously. Observe that all δ_{1+}^i, δ_{1-}^i, δ_{2+}^i, δ_{2-}^i measure the distance between a curve and its osculating circle and define

$$\delta^i = \max(\delta_{1+}^i, \delta_{1-}^i, \delta_{2+}^i, \delta_{2-}^i). \tag{14}$$

Since the curve's parametric length is of $\mathcal{O}(h_i)$ and the osculating circle is a second order approximation to the curve, Taylor expansion gives $\delta = \mathcal{O}(h_i^3)$.

Finally, consider osculating circles c_1^i, c_2^i of both curves at intersection point P and define two fat arcs $\mathcal{FA}_1^i$, $\mathcal{FA}_2^i$ arisen from c_1^i, c_2^i by adding/subtracting the offsetting distance δ^i, see Fig. 5(b).

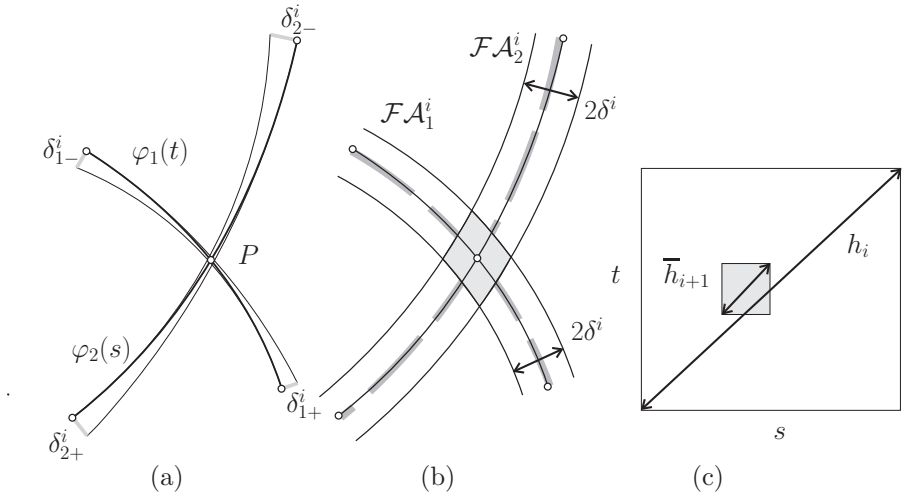

Figure 5: (a) Spirals φ_1 and φ_2 are transversally intersected at point P. δ^i_{1-} (thick grey) is the distance between the startpoint of φ_1 and the osculating circle at its endpoint and it bounds the distance between φ_1 and its lower envelope. (b) Osculating circles c^i_1 and c^i_2 (dashed grey) of both curves at P define skeletons of fat arcs $\mathcal{FA}^i_1$, $\mathcal{FA}^i_2$ of width $2\delta^i$, $\delta^i = \max(\delta^i_{1-}, \delta^i_{1+}, \delta^i_{2-}, \delta^i_{2+})$. $\mathcal{FA}^i_1$ ($\mathcal{FA}^i_2$) is the supersets of $\mathcal{SFA}^i_1$ ($\mathcal{SFA}^i_2$), and consequently its intersection (grey domain) is a superset of the region generated in line 9 of Algorithm 1. (c) In the parametric st-space, h_i is the original diameter, whereas $\overline{h}_{i+1}$ corresponds to the restriction of both curves to $\mathcal{FA}^i_1 \cap \mathcal{FA}^i_2$.

These fat arcs are supersets of $\mathcal{SFA}$ regions constructed in the i-th iteration of `SpiralClipping`, see line 9 of Algorithm 1. Hence the diameter h_{i+1} of the parametric subspace generated in the $(i+1)$-th iteration of Algorithm 1 is bounded by $\overline{h}_{i+1}$, the diameter of the subspace that corresponds to the restriction of φ_1, φ_2 to $\mathcal{FA}^i_1 \cap \mathcal{FA}^i_2$. Lemma 3 gives $\operatorname{diam}(\mathcal{FA}^i_1 \cap \mathcal{FA}^i_2) = \mathcal{O}(h^3_i)$. Since the error is of the same order $\mathcal{O}(h^3_i)$ both in the model and in the parametric space, we obtain $\overline{h}_{i+1} \leq \mathcal{O}(h^3_i)$, which completes the proof. □

Remark 4. In a special case, when the intersection point P is an inflection point on one the input curves, Algorithm 1 considers the limit $\mathcal{SFA}$s whose upper envelopes consists of two line segments, see Fig. 3(a). In such a case, the approximation order is two and so is the convergence rate.

4. Examples

In this section, we present several examples of computing the intersection points between two planar parametric curves using bounding $\mathcal{SFA}$ regions. All examples were created with aid of the Irit[1] solid modeling environment, where

[1] www.cs.technion.ac.il/∼irit

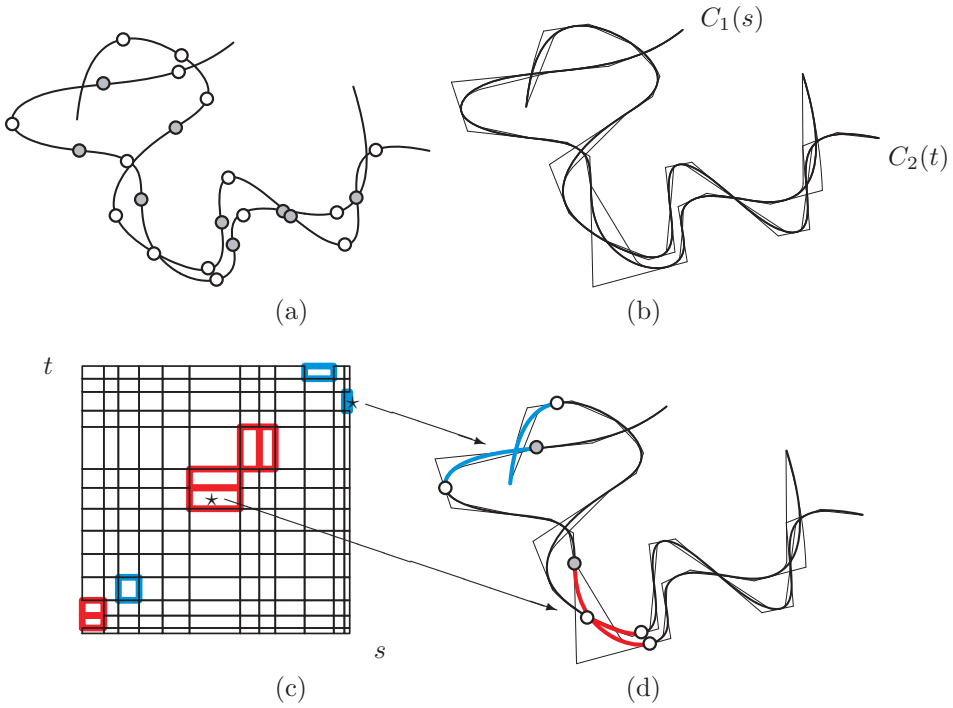

Figure 6: (a) Preconditioning step of Algorithm 2: both curves are split at points of extremal curvature (white dots) and inflection points (grey). (b) All segments are provided by their $\mathcal{SFA}$ regions and spiral clippings, see Algorithm 1, are applied. (c) The segmentation of the parametric st-space, with domain's classification of three kind: $\mathcal{SFA}$ regions with empty intersection (white), transversal intersection guaranteeing exactly one intersection point (blue) and non-transversal intersections (red) are displayed. Only the red domains need to be subdivided in the second iteration of Algorithm 2. (d) Two pairs of segments, one with transversal (blue) and the second one with non-transversal intersection (red) are highlighted. Their corresponding domains are provided by asterisks.

the presented algorithm is implemented. All presented examples have been tested on a PC with an Intel(R) Pentium(R) CPU (2.8GHz), 1GB of RAM. Table 1 shows the parameters and timings for examples shown in Figs. 6–8.

Algorithm 2 was compared with a subdivision based curve-curve intersecting algorithm which exploits the single solution test of [17]. In this very efficient implementation, skewed bounding boxes are also used to detect and eliminate the no-intersecting segments. If (at most) a single intersection point is guaranteed by [17], a numerical improvement stage, e.g. Newton-Raphson, is applied.

Two curves, transversally intersected at seven distinct locations, are shown at Fig 6(b). The preprocessing step of Algorithm 2 is depicted at Fig 6(a) and the corresponding segmentation of the parametric st-space is depicted at (c). Another example of two closed B-spline curves with complex topology is shown

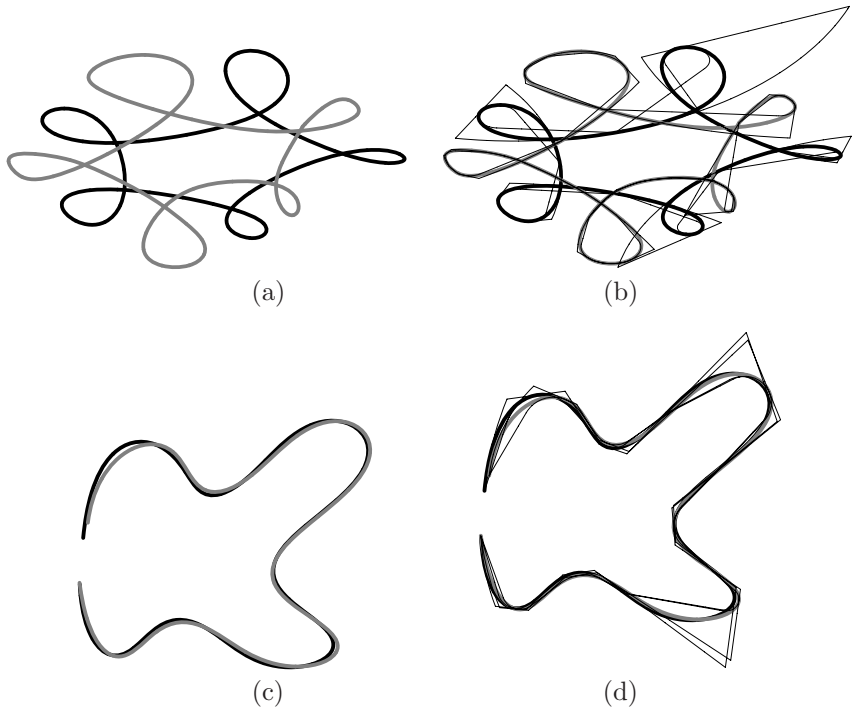

Figure 7: (a) Two closed quartic B-spline curves with 10 transversal intersections are shown. They are segmented and bounded by sets of $\mathcal{SFA}$s (b). (c) A numerical noise was applied on the control points of a cubic B-spline curve yielding an almost-identical configuration. (d) All the initial $\mathcal{SFA}$s of the subregions with the high proximity are overlapping.

at Fig. 7(a). Both curves possess several loops which makes the preprocessing step the most time demanding part of Algorithm 2, see Table 1.

A more challenging example is shown at Fig. 7(c), where one curve was created from another by applying some numerical noise on its control points. Such a configuration makes it difficult to decide between a 'no-root" and 'may-be-root" case and typically requires a large number of subdivisions. In contrast, one should observe the low number of subdivisions required by Algorithm 2, in Table 1.

Another example is shown at Fig. 8, where both curves possess a tiny loop. In such a case, if the subdivision tolerance is not sufficiently fine, an inexact number of roots might be returned by any subdivision based solver. In contrast, Algorithm 2 prevents this phenomenon by splitting both loops and handling loop-free spiral segments.

Table 1 offers the number of subdivisions, total number of all iterations and timings, of both algorithms. In the case of Algorithm 2, timings are reported separately for the preprocessing step that divides a general curve into spirals

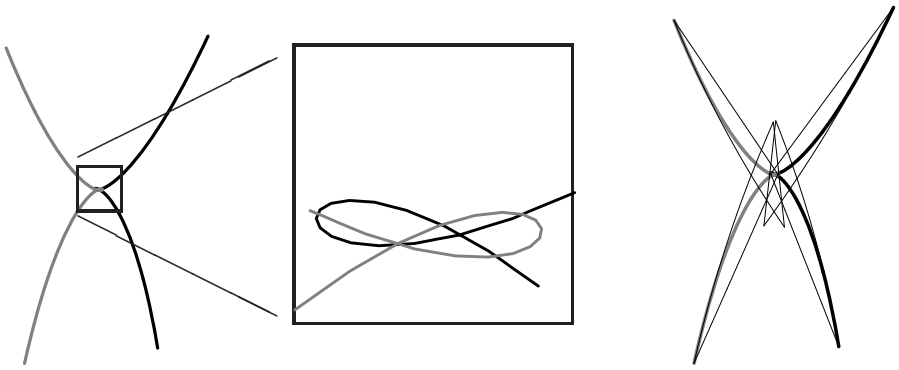

Figure 8: (a) Two Bézier curves of degree four, each provided with a tiny loop. (b) A zoom-in on the loop region. (c) Each curve is split into two spirals and bounded by $\mathcal{SFA}$s.

Table 1: Statistics on the presented CCI examples of Algorithm 2 and its comparison to a subdivision based algorithm with single solution test of [17] for a numerical tolerance $\varepsilon = 10^{-6}$ over normalized parametric st-spaces: I indicates the number of intersection points. Further, the number of subdivisions, total number of all iterations and timings of both algorithms are displayed. Every example was executed 1000 times and the timings were averaged.

Example	I	Algorithm 2				Algorithm [17]		
		subd	iter	$T_{prep}(sec)$	$T_{clip}(msec)$	subd	iter	$T(msec)$
Fig. 6	7	*25*+6	199	0.54	0.78	35	141	0.68
Fig. 7 (a)	10	*20*+4	416	12.6	1.21	55	221	1.41
Fig. 7 (c)	9	*28*+12	247	3.73	1.33	127	509	2.61
Fig. 8	6	*2*+14	67	0	0.54	23	93	0.25

and the clipping stage that is accomplished by `SpiralClipping`. Also, the total number of subdivisions (the third column) is reported as a sum of the preprocessing subdivisions (italics) and those required by the invocations of `SpiralClipping`.

Observe the comparison of Algorithm 2 with the one based on [17], see Table 1. Whereas the preconditioning stage is time demanding, once the original curves are split into spiral segments, `SpiralClipping` offers favorable results.

5. Conclusion

A bounding region of a planar spiral curve, denoted *spiral fat arc*, was introduced. This bounding region, delimited by two circular arcs and two lines, is a

second order approximation to the original curve and it guarantees the curve inside it is self-intersection free. Exploiting spiral fat arcs, a simple-to-implement CCI algorithm was also presented. In the case of a transversal intersection, its cubical convergence rate towards the intersection point was shown. As a future work, an improvement of the trimming stage, as well as the implementation of the tangential case (when two $\mathcal{SFA}$s overlap) might be addressed. Testing other applications of spirals with the help of $\mathcal{SFA}$s is also within the scope of our interest.

6. Acknowledgments

This research was partly supported by the Israel Science Foundation (grant No. 346/07), and in part by the New York metropolitan research fund, Technion.

References

[1] G. Harary and A. Tal. 3D Euler spirals for 3D curve completion. *ACM Symposium on Computational Geometry*, 2010.

[2] Bartoň M. Quadratic clipping and its generalization for polynomial systems. PhD thesis, Charles University, Prague, 2007.

[3] Bartoň M., Jüttler B. Computing roots of systems of polynomials by linear clipping, Technical Report 2007-18, SFB F013 Technical Report, August 2007. Available at http://www.sfb013.uni-linz.ac.at.

[4] Moore B., Jüttler B. A quadratic clipping step with superquadratic convergence for bivariate polynomial systems, Technical Report 2008-78, FSP Technical Report, October 2008.

[5] S. Béla and B. Jüttler. Fat arcs for implicitly defined curves. Proceedings of *Mathematical Methods for Curves and Surfaces*, LNCS, Springer, pp. 26-40, 2009.

[6] A. Cohen, R. Riesenfeld, G. Elber. *Geometric modeling with splines*. A K Peters, Massachusetts, 2001.

[7] D. A. Dietz, B. Piper, E. Sebe. Rational cubic spirals. *Computer Aided Design*, Vol. 40, pp. 3-12, 2008.

[8] G. Elber. Symbolic and Numeric Computation in Curve Interrogation. *Computer Graphics forum*, Vol. 14, pp. 25–34, 1995.

[9] I. Hanniel and G. Elber. Subdivision termination criteria in subdivision multivariate solvers using dual hyperplanes representations. *Computer Aided Design*, Vol. 39, pp. 369–378, 2007.

[10] T. W. Sederberg, S. C. White and A. K. Zundel. Fat arcs: A bounding region with cubic convergence. *Computer Aided Geometric Design*, Vol. 6, pp. 205-218, 1989.

[11] G. Farin. Class A Bézier curves. *Computer Aided Geometric Design*, Vol. 23, pp. 573-581, 2006.

[12] A. Kurnosenko. Applying inversion to construct planar, rational spirals that satisfy two-point G^2 Hermite data. *Computer Aided Geometric Design*, Vol. 27, pp. 262-280, 2010.

[13] R. L. Levien. From spiral to spline: Optimal techniques in interactive curve design PhD thesis, University of California, Berkeley, 2009.

[14] R. L. Levien and C. H. Sequin. Interpolating splines: Which is the fairest of them all? *Computer Aided Design and Applications*, Vol. 4, pp. 91-102, 2009.

[15] Y. Mineur, T. Lichah, J. M. Castelain, H. Giaume. A shape controlled fitting method for Bézier curves. *Computer Aided Geometric Design*, Vol. 15, pp. 879-891, 1998.

[16] T. W. Sederberg. Curve intersection using Bézier clipping. *Computer Aided Design*, Vol. 22, pp. 538-549, 1990.

[17] T. W. Sederberg and R. J. Meyers. Loop detection in surface patch intersection. *Computer Aided Geometric Design*, (5):161–171, 1988.

[18] Ch. Schulz. Bézier clipping is quadratically convergent. *Computer Aided Geometric Design*, Vol. 26, pp. 61-74, 2009.

[19] N. Yoshida, R. Fukuda and T. Saito. Log-aesthetic space curve segments. *ACM Symposim on Solid and Physical Modeling*, San Francisco, pp. 35-46, 2009.

[20] D. J. Walton and D. S. Meek. G^2 curve design with a pair of Pythagorean Hodograph quintic spiral segments. *Computer Aided Geometric Design*, Vol. 24, pp. 267-285, 2007.

[21] D. J. Walton and D. S. Meek. Planar spirals that match G^2 Herimete data. *Computer Aided Geometric Design*, Vol. 15, pp. 103-126, 1998.

[22] Z. Yao. A novel cutter path planning approach to high speed machining. *Computer-Aided Design and Applications*, Vol. 3, pp. 241–248, 2006.

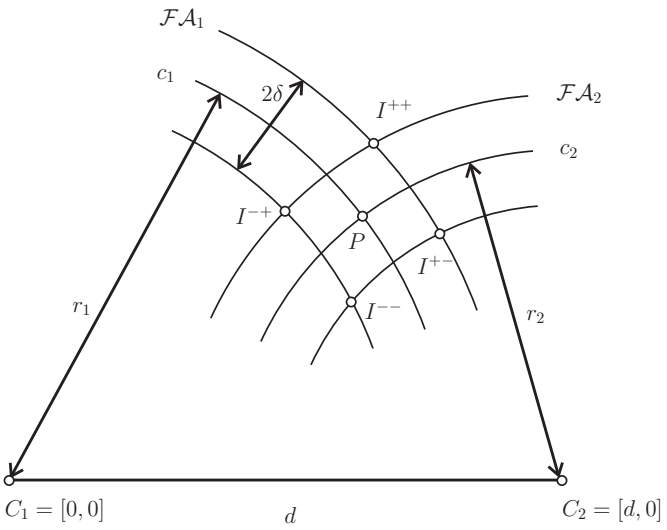

Figure 9: Circles c_1 and c_2 are transversally intersected at P and so are the associated fat arcs $\mathcal{FA}_1$ and $\mathcal{FA}_2$, both of width 2δ. The diameter of its intersection is bounded from above by $2\max\{\|PI^{ij}\|\}$, $i,j = +,-$, and all the distances $\|PI^{ij}\|$, $i,j = +,-$, are bounded from above by a linear function in δ.

7. Appendix

Proof of Lemma 3. We recall S is one of the connected components of $\mathcal{FA}_1 \cap \mathcal{FA}_2$. Let us denote I^{ij}, $i,j = +,-$, the corner points of S, see Fig. 9. Since the diameter of S is bounded from above by $2\max\{\|PI^{ij}\|\}$, $i,j = +,-$, only the distance $\|PI^{ij}\|$ needs to be considered. We show that $\|PI^{ij}\|$ is bounded from above by some distance function which is linear in δ.

Without loss of generality, C_1 is at the origin, $C_1 = [0,0]$, and C_2 lies on the positive x-axis, $C_2 = [d,0]$. Let $P = [x,y]$, $x,y > 0$, be the intersection point of c_1 and c_2 and consider its coordinates x and y as functions of δ when circle's radii are increased/decreased by δ. It holds

$$\begin{aligned} x^2 + y^2 &= r_1^2, \\ (d-x)^2 + y^2 &= r_2^2, \end{aligned} \tag{15}$$

by eliminating y^2 we directly obtain

$$x = \frac{r_1^2 - r_2^2 + d^2}{2d}, \tag{16}$$

and consequently x is linear in δ for $r_i \to r_i \pm \delta$, $i = 1,2$. Since

$$y = \sqrt{r_1^2(\delta) - x^2(\delta)} = \sqrt{a\delta^2 + b\delta + c} \tag{17}$$

for some $a,b,c \in \mathbb{R}, c > 0$, y is bounded from above by a linear function in δ (a tangent line of the graph of function y at $\delta = 0$). Hence the coordinates

of all I^{ij}, $i, j = +, -$, are bounded from above by linear functions in δ and consequently $\mathrm{diam}(S) = \mathcal{O}(\delta)$. $\square$